J. Phys. D: Appl. Phys. **31** (1998) 925–941. Printed in the UK PII: S0022-3727(98)71753-X

REVIEW ARTICLE

Biquadratic interlayer coupling in layered magnetic systems

S O Demokritov

Fachbereich Physik, Universität Kaiserslautern, 67663 Kaiserslautern, Germany

Received 25 March 1997

Abstract. An unusual interlayer coupling, recently discovered in layered magnetic systems, is analysed from the experimental and theoretical points of view. This coupling favours the 90° orientation of the magnetization of the adjacent magnetic films. It can be phenomenologically described by a term in the energy expression, which is biquadratic with respect to the magnetizations of the two films. The main experimental findings, as well as the theoretical models, explaining the phenomenon are discussed.

1. Introduction

Since the discovery of the antiferromagnetic interlayer coupling in layered magnetic systems in 1986 [Gru86] it was naturally implied that this interaction is of the Heisenberg type. Therefore the energy expression describing two coupled magnetic layers was written as follows [Gru91]

$$E_{\text{int}} = -2A_{12}(\boldsymbol{m}_1 \cdot \boldsymbol{m}_2) = -J_1(\boldsymbol{m}_1 \cdot \boldsymbol{m}_2) \qquad (1.1)$$

where E_{int} is the energy per surface unit area of the interface and $\boldsymbol{m}_1$ and $\boldsymbol{m}_2$ are the *unit* magnetization vectors of the first and the second magnetic layers respectively. Note here, that in recent publications the definition of the coupling strength with $J_1(= 2A_{12})$ is mainly in use. According to the general agreement the positive (negative) sign of the factor J_1 corresponds to the ferromagnetic (antiferromagnetic) type of the interaction. Since equation (1.1) is bilinear with respect to $\boldsymbol{m}_1$ and $\boldsymbol{m}_2$, such a type of interaction is called a bilinear one. Together with the Zeeman energy and the crystallographic anisotropy energy equation (1.1) is the basis for the analysis of the magnetic properties of such layered systems.

The general formula describing the total energy is straightforward, but very complex, especially in the case of arbitrary orientations of the applied field and easy axes of contributing anisotropies. To illustrate the salient features we discuss here first the case of two magnetic layers with the same magnetization M_0 and the same thickness t. The anisotropy contribution is taken as a fourfold one, which is the dominating anisotropy term in Fe(001) films and it is described here by the anisotropy constant K_4 ($K_4 = 4.5 \times 10^4$ J m^{-3} for Fe). Moreover, if the magnetic field is applied in the plane of the film surface (xy-plane) along an easy axis (x-axis), then the total energy expression is written as

$$E_{\text{tot}} = -M_0 t(m_{1x} + m_{2x})H + K_4 t(m_{1x}^2 m_{1y}^2 + m_{2x}^2 m_{2y}^2) - J_1(\boldsymbol{m}_1 \cdot \boldsymbol{m}_2). \qquad (1.2)$$

For a given external field the minima of equation (1.2) yield the orientations of $\boldsymbol{m}_1$ and $\boldsymbol{m}_2$ and thus the components of the total magnetization along any direction. For positive J_1, even in zero field, $\boldsymbol{m}_1$ is parallel to $\boldsymbol{m}_2$ and nothing significant happens with increasing field. For negative J_1 the energetic minimum is achieved at $H = 0$, if $\boldsymbol{m}_1$ is antiparallel to $\boldsymbol{m}_2$ and the reorientation transition takes place with increasing field. For example, for $|J_1| \gg K_4 t$ a theoretical analysis predicts a second-order reorientation transition and a smooth linear $M(H)$-dependence, followed by the saturation. The saturation field H_S can be determined via the following relation

$$H_S = -\frac{2J_1}{M_0 t}. \qquad (1.3)$$

On the other hand, for $|J_1| \ll K_4 t$, the magnetization increases slowly in small fields, but then at some critical field H_S the system undergoes the first-order transition with an abrupt jump to the saturation magnetization. The saturation field H_S in this case is written as

$$H_S = -\frac{J_1}{M_0 t}. \qquad (1.4)$$

The experimental magnetization curves shown in figure 1 illustrate the described behaviour. The full curves are calculated on the basis of equation (1.2).

If $|J_1|$ has the same order of magnitude as $K_4 t$, it is not possible to derive an analytical expression similar to equations (1.3) or (1.4), and a numerical procedure is needed to find the orientations of $\boldsymbol{m}_1$ and $\boldsymbol{m}_2$ as a function of the field. The results of such calculations are quite

0022-3727/98/080925+17$19.50 © 1998 IOP Publishing Ltd

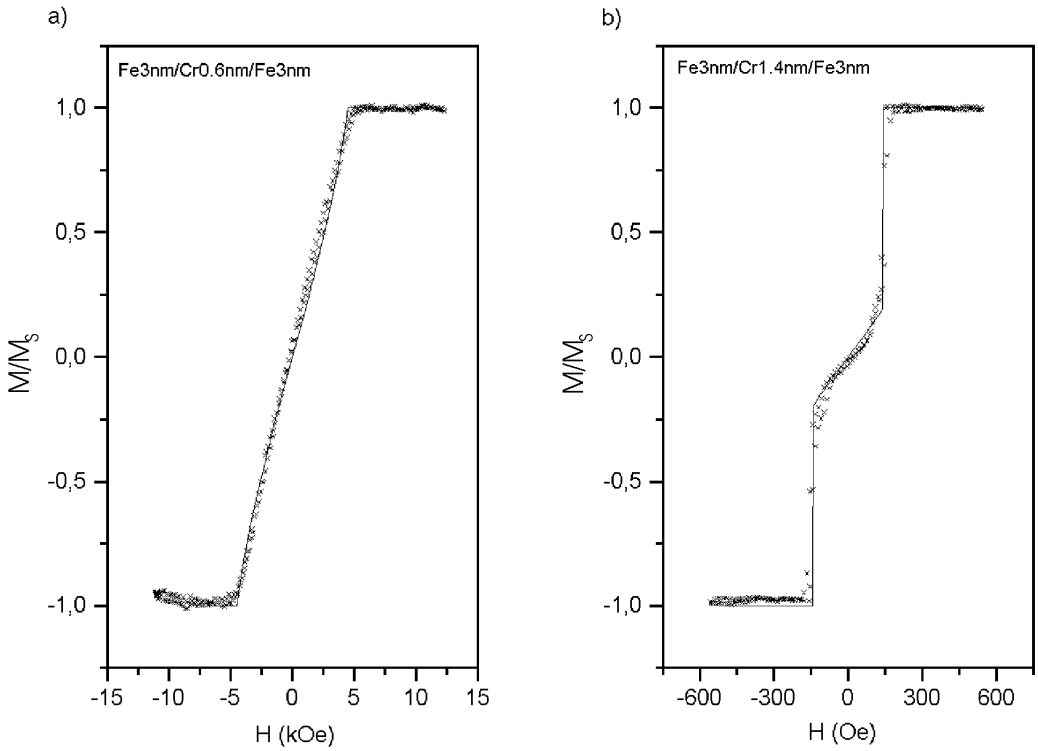

Figure 1. Component of the magnetization of the Fe (3 nm)/Cr, t_{Cr}/Fe(001)(3 nm) layered system, parallel to the applied magnetic field plotted as a function of the field: (*a*) t_{Cr} = 0.6 nm, (*b*) t_{Cr} = 1.4 nm. The field is applied along [100] (easy axis). The full curves are numerically calculated on the basis of equation (1.2) with $K_4 t$ = 0.13 mJ m^{-2} and J_1 = 1.54 mJ m^{-2} (*a*), J_1 = 0.07 mJ m^{-2} (*b*).

obvious: the height of the jump decreases with increasing $|J_1|/K_4 t$ ratio, and at some value of this parameter the jump disappears and the transition becomes the second-order transition [Koe92].

However, a very different situation was found in the experiment for some Fe/Cr/Fe trilayers. The magnetization curves of the Fe/Cr/Fe(001) layered system, measured for relatively thick Cr spacers (t_{Cr} > 2–3 nm) demonstrate a well-defined phase, existing in a finite interval of the field. In this phase the component of the total magnetization of the trilayer, parallel to the field, equals to *one-half* of the saturation magnetization [Gru91]. For some t_{Cr} the phase already exists at zero field; for some t_{Cr} it is an intermediate phase between the phase with antiparallel alignment of two magnetizations and the saturated state (see figure 2). Detailed investigations of the Fe/Cr/Fe layered system by means of the magneto-optical Kerr effect (MOKE) microscopy and vector MOKE magnetometry were performed by Ruehrig *et al* [Rue91]. The domain patterns of Fe(10 nm)/Cr(0.5 nm)/Fe(10 nm) in remanence and their interpretation are shown in figure 3. It is worth noting here once more that the fourfold symmetry of Fe(001) films brings about four easy axes in the (001)-plane, therefore all magnetization vectors of the individual magnetic layers shown in figure 3 are directed along easy axes. One can see in figure 3 that the magnetization of each layer can be oriented along any easy axis in different domains, but in all domains the two layers prefer to be magnetized at 90° to each other, rather than to be parallel or antiparallel to each other. The vector MOKE magnetometry reveals the fact that the component of the total magnetization, which is perpendicular to the field, exists in this phase. This transverse magnetization component is much smaller than the parallel one and it is highly hysteretic.

Both domain structures obtained by MOKE microscopy and the magnetization curves discussed above are not consistent with results derived using equation (1.2). Therefore, the additional non-collinear interlayer coupling was phenomenologically introduced in the following form [Rue91]

$$E_{\text{int}} = -2A_{12}(\boldsymbol{m}_1 \cdot \boldsymbol{m}_2) - B_{12}(\boldsymbol{m}_1 \cdot \boldsymbol{m}_2)^2. \qquad (1.5)$$

In later publications in a similar way as A_{12}, B_{12} was substituted by another parameter $J_2 = B_{12}$:

$$E_{\text{int}} = -J_1(\boldsymbol{m}_1 \cdot \boldsymbol{m}_2) - J_2(\boldsymbol{m}_1 \cdot \boldsymbol{m}_2)^2. \qquad (1.6)$$

We will be using this definition later in this paper, although both sets of notation can be found in the literature. The second term in equation (1.6) is called biquadratic coupling, since it is biquadratic with respect to $\boldsymbol{m}_1$ and $\boldsymbol{m}_2$. As is easily seen from equation (1.6), this interaction, if it dominates, favours the orientation where $\boldsymbol{m}_1 \cdot \boldsymbol{m}_2 = 0$ (90° phase), providing that $J_2 < 0$.

Heinrich *et al* [Hei91] have considered the angular-dependent bilinear coupling parameter J_1^* for the explanation of their FMR experiments in Co/Cu/Co trilayers:

$$J_1^* = j_x + j_1(1 - \boldsymbol{m}_1 \cdot \boldsymbol{m}_2) \qquad (1.7)$$

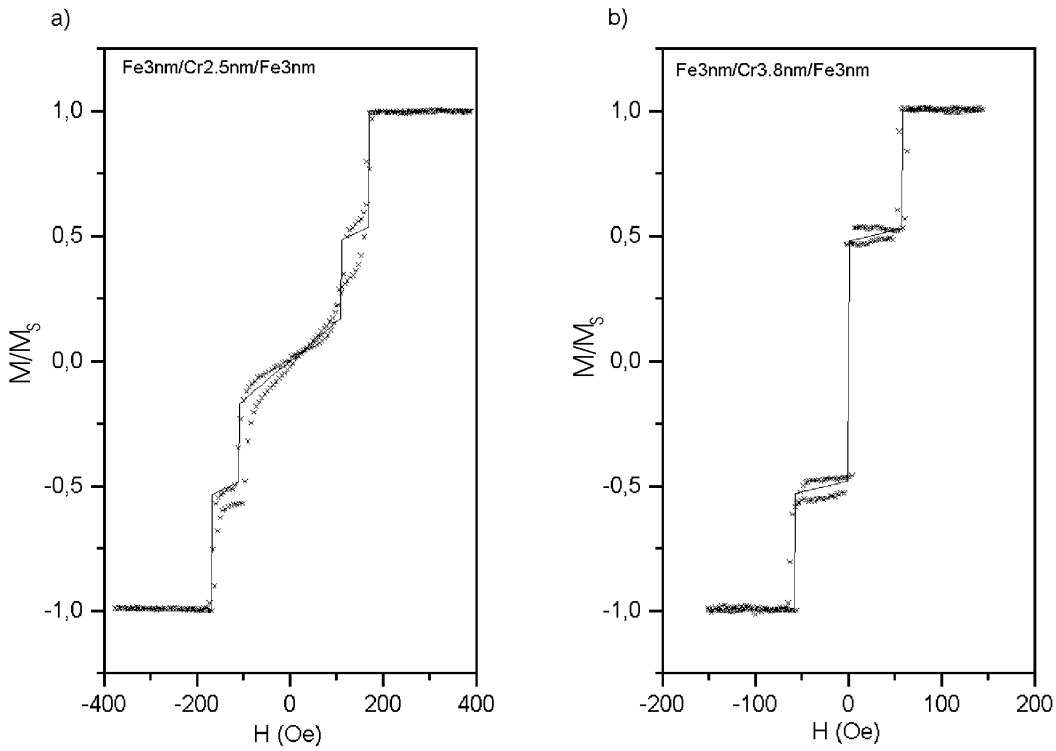

Figure 2. Component of the magnetization of the Fe (3 nm)/Cr, t_{Cr}/Fe(001)(3 nm) layered system, parallel to the applied magnetic field plotted as a function of the field: (*a*) t_{Cr} = 2.5 nm, (*b*) t_{Cr} = 3.8 nm. The field is applied along [100] (easy axis). The full curves are calculated on the basis of equation (1.6) with $K_4 t$ = 0.13 mJ m^{-2} and J_1 = 0.07 mJ m^{-2}, J_2 = 0.012 mJ m^{-2} (*a*) and $J_1 + J_2$ = 0.03 mJ m^{-2} (*b*).

this is, however, equivalent to the definition introduced in equation (1.6), if $J_1 = j_x + j_1$ and $J_2 = -j_1$.

The biquadratic term was included in equation (1.6) in a scalar form, although contrary to the bilinear coupling it is not the only term allowed even in the systems possessing the tetragonal symmetry (e.g. layered systems on the basis of Fe(001) films). The phenomenological analysis performed by Demokritov *et al* [Dem98] shows that two additional anisotropic biquadratic terms are allowed even in this high symmetrical case. The magnetization curves, calculated for a system with such an anisotropic biquadratic coupling, differ dramatically from those corresponding to layered systems with the isotropic coupling. Later in this paper the term biquadratic coupling will describe the isotropic biquadratic coupling.

To conclude the introduction, let us note the fact that the formulae discussed so far all apply to trilayers, i.e. two magnetic films, separated by a spacer. In the case of multilayers with a very large number of magnetic layers all but the outer films have two interacting neighbours, instead of only one, as in the case of a trilayer. Therefore we need to modify the equations valid for multilayers by simply replacing in the previous equations J_1 and J_2 by $2J_1$ and $2J_2$. As a result, for example, under otherwise identical conditions the saturation field of such a multilayer in the presence of antiferromagnetic or 90° coupling should be increased by a factor of two as compared with the saturation field of a trilayer.

2. Phenomenological analysis

In this section we consider the consequences of the introduction of biquadratic coupling brings about. Depending on the type and values of the contributing anisotropies and the interlayer coupling, magnetic trilayers can demonstrate four (two collinear and two non-collinear) different phases, which are classified as follows:

(i) parallel phase ($\boldsymbol{m}_1 \cdot \boldsymbol{m}_2 = 1$, maximum total magnetization M_S);

(ii) antiparallel phase ($\boldsymbol{m}_1 \cdot \boldsymbol{m}_2 = -1$, zero total magnetization);

(iii) 90° phase ($\boldsymbol{m}_1 \cdot \boldsymbol{m}_2 = 0$, total magnetization has two components parallel to $\boldsymbol{m}_1$ and to $\boldsymbol{m}_2$, which are both equal to $M_S/2$);

(iv) canted phase ($\boldsymbol{m}_1$ and $\boldsymbol{m}_2$ form an arbitrary angle).

As has already been mentioned, the biquadratic coupling causes a non-collinear alignment of the magnetizations only in the case when $J_2 < 0$. Otherwise it favours the collinear alignment. Since the energy contribution of the biquadratic coupling to the parallel and antiparallel alignments is the same, its influence in this case on the magnetic properties of the system is minimal.

The in-plane anisotropy affects dramatically the magnetic properties of layered systems with biquadratic coupling. If the anisotropy is negligible, the resulting magnetic configuration can easily be derived from equation (1.6). If $J_2 < 0$ and $2|J_2| > |J_1|$, the magnetization

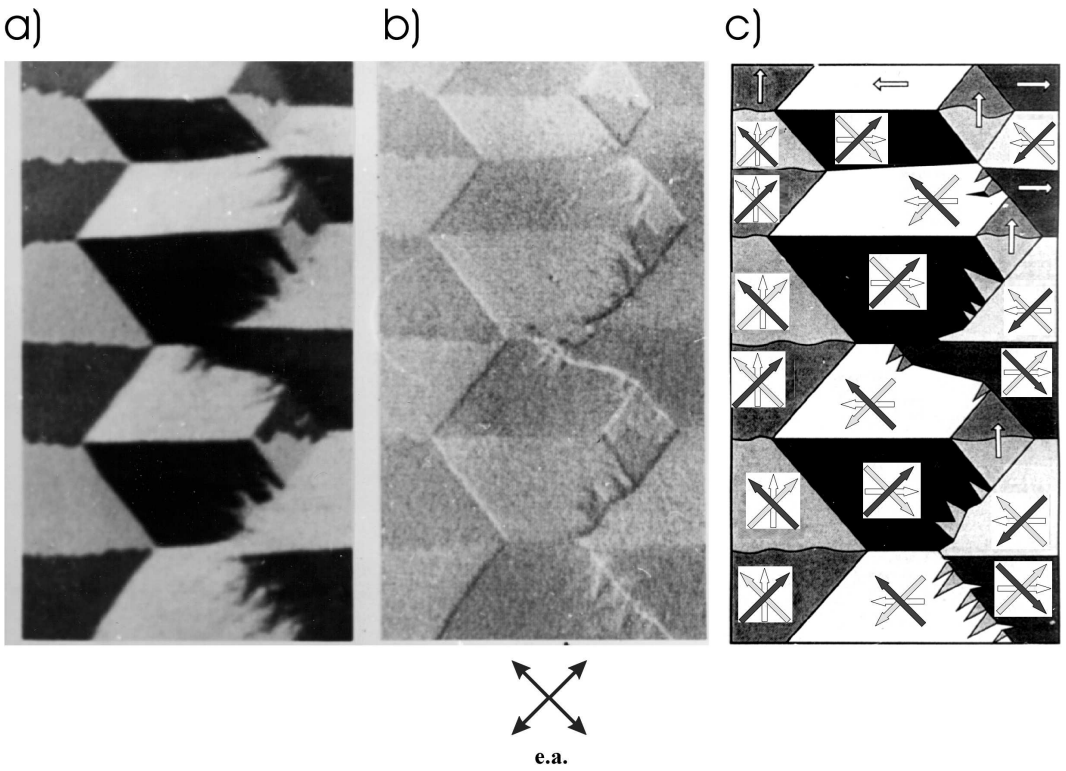

Figure 3. (*a*), (*b*) Examples of the domain pattern of the Fe(001)(10 nm)/Cr(001)(0.5 nm)/Fe(001)(100 nm) layered system in remanence, measured by Kerr microscopy, obtained in the different polarization arrangements. (*c*) Interpretation, consistent with all observed patterns. The symbols indicate the net magnetization by the open arrows, the magnetization of the top layer by the black arrows and of the bottom layer by the gray arrows. The arrows in the middle of the figure indicate the directions of the four possible easy axes of each layer (from [Rue91]).

of two films is canted even at zero field, and the canting angle φ between $\boldsymbol{m}_1$ and $\boldsymbol{m}_2$ (for both ferromagnetic (FM) and antiferromagnetic (AF) type of J_1) is determined as follows:

$$\cos\varphi = -\frac{J_1}{2J_2}. \tag{2.1}$$

With increasing applied magnetic field the canting angle decreases and at H_S

$$H_S = -\frac{2}{M_0 t}(2J_2 + J_1) \tag{2.2}$$

saturation is reached.

It is also obvious that the uniaxial anisotropy with the same easy axes for both films diminishes the influence of the biquadratic coupling, because in the canted phase one of the magnetization vectors is not aligned along the easy axis and therefore the total energy of the canted phase increases.

A fourfold in-plane anisotropy does not suppress the non-collinear phases. On the other hand, it corresponds to a typical experimental situation, when a layered system on the basis of Fe(001) magnetic film is under investigation. Therefore, we consider this case in detail. As can be seen below, typical values of J_2 are of the order of 0.01–0.1 mJ m^{-2}. For typical thicknesses of magnetic films (t = 5–10 nm) the parameter $K_4 t$ is large compared with J_2. This makes the analysis relatively simple. In fact, if the anisotropy dominates, the only possibility for $\boldsymbol{m}_1$ and $\boldsymbol{m}_2$ is to be aligned along one of the four easy axes. Since any deviation of $\boldsymbol{m}_1$ or $\boldsymbol{m}_2$ from the easy axes causes significant increase in energy, such deviations are not permitted. Thus, the system cannot be in the canted phase with an arbitrary angle. Only three possible phases, parallel phase, antiparallel and 90° phase, are allowed. In a similar way to what is usually done for the (H, T) coordinates, the phase diagram of the system can be considered in the (J_1, J_2) phase space [Rue91]. Such a phase diagram is shown for $H = 0$ in figure 4. In contrast to the diagram discussed in [Rue91], this diagram contains *two* antiparallel phases. The first one (AP1), corresponding to positive values of J_2 is a completely collinear phase. The transition from the antiparallel to the parallel orientation with increasing applied field takes place without any intermediate phase. The second antiparallel phase (AP2), corresponding to negative values of J_2, passes through an intermediate 90° orientation, which is followed by the saturation. Another phase shown in figure 4 is a 90° phase. It exists at both positive and negative values of J_1. Its magnetization process is quite simple: at some critical field the system jumps into the parallel (P) phase.

The phase diagram presented in figure 4 corresponds to a zero applied field. Let us consider in detail the magnetization processes of the AP2 phase, in the case when the field is applied along an easy axis. From a simple energy minimization procedure, the values of the transition field H_{S1} (transition from the AP2 phase to the 90° phase) and H_{S2} (transition from the 90° phase to the P phase) can

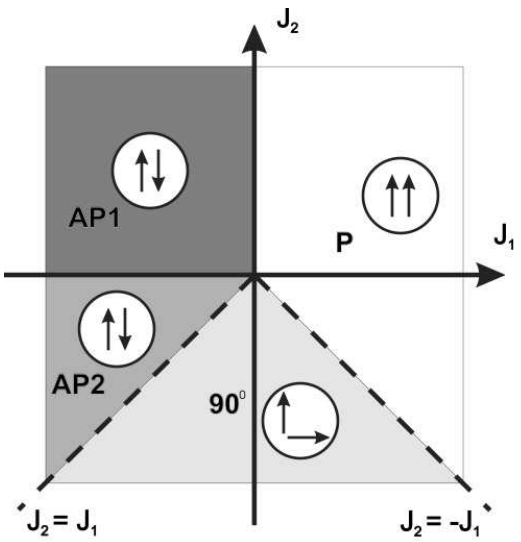

Figure 4. Phase diagram of two equivalent coupled magnetic layers at zero applied field in (J_1, J_2) coordinates for the case of a dominating fourfold anisotropy. Note the existence of two antiparallel phases, which undergo different orientation phase transitions with increasing applied field.

be analytically derived on the basis of equation (1.6), if $|J_1|, |J_2| \ll K_4 t$:

$$H_{S1} = -\frac{J_1 - J_2}{Mt} \tag{2.3}$$

$$H_{S2} = -\frac{J_1 + J_2}{Mt}. \tag{2.4}$$

Between these two fields one observes a plateau in the magnetization curve, corresponding to half of the value of the saturation magnetization. As implied above, a negative value of H_S means that a corresponding transition does not take place in reality. For example, if J_1, $J_2 < 0$ and $|J_1| < |J_2|$ (this corresponds to the 90° phase in figure 4) the transition field $H_{S1} < 0$ and the antiparallel phase does not exist at all. In this case the remaining transition field H_{S2} describes the transition from the 90° phase to the P phase. Equations (2.3) and (2.4) give a straightforward possibility of determining experimentally the values of J_1 and J_2 by measuring H_{S1} and H_{S2}. It is also clear from the above discussion that this method does not work if the ground state at zero field is the 90° phase. In this case only one measured value (H_{S2}) is available for the determination of both J_1 and J_2.

A phase diagram similar to that shown in figure 4 can also be obtained in the general case without the restrictions $|J_1|, |J_2| \ll K_4 t$. This was done by Maccio *et al* for two magnetic monolayers on the basis of quantum mechanics [Mac94]. However one needs complicated calculations to obtain such a diagram. We do not intend to go into details. Just one point should be mentioned here: in addition to the phases already discussed a canted phase appears in this diagram. This means that the bilinear and biquadratic couplings can create a canted phase in a system with a modest in-plane anisotropy.

The above analysis was performed without taking into account thermal fluctuation, because due to the *intralayer* exchange in ferromagnetic films these fluctuations are suppressed. One can consider the magnetization vector of every film as a temperature-dependent variable, which is described by a slowly changing function of the coordinates along the film. For the same reason we did not take into account the variation of the magnetization across magnetic films. That is possible if the thickness of the film does not exceed a so-called exchange length, which is about 50 nm for Fe.

3. Experiment

3.1. Experimental techniques

In this section a short description of the experimental techniques used for the investigation of the magnetic properties of layered magnetic systems is presented. One can divide these methods in two groups: static measurements (static magnetometry, domain observation), which provide information about the angle between the magnetizations of different magnetic layers and its field dependence, and dynamic techniques (ferromagnetic resonance, inelastic light scattering), which are connected to the frequencies of spin wave modes in the layered systems. A comparison of the experimental dependences with the calculated curves gives the opportunity to derive the strength and the type of the coupling.

We will discuss the advantages and disadvantages of every technique. This section should facilitate the understanding of the experimental results, described in the following sections.

3.1.1. Static magnetometry. The interlayer coupling in general and the biquadratic coupling in particular can be studied by measuring the field dependence of the direction and value of the macroscopic magnetic moment of the sample. There are various techniques which provide this information, such as magneto-optical Kerr effect (MOKE) magnetometry, vibrating sample magnetometry (VSM), superconducting quantum interference device (SQUID) magnetometry, alternating gradient magnetometry (AGM), etc.

The magneto-optical Kerr effect is the change in the polarization state (the polarization plane and the ellipticity) of light by reflection at the surface of magnetic materials. This change originates from a difference in the complex Fresnel reflection coefficients for left and right circularly (or vertically and horizontally linearly) polarized light. The difference is only present for a non-zero magnetization, and its magnitude is determined by the different magnetization components. There are three high-symmetry configurations used in MOKE measurements, which are called the polar, the longitudinal and the transverse MOKE. For example, the polar MOKE is sensitive to the out-plane magnetization component, whereas the longitudinal one is sensitive to the in-plane magnetization component. Using all three configurations one can in principle measure all three magnetization components. A typical value of the

penetration depth of light in metals is about 10–20 nm. This means, for example, for a sample containing two magnetic layers, that the contributions of each magnetic layer to the MOKE signal are different if the thicknesses of the individual layers are within the interval of 10–20 nm. Using this fact one can monitor the magnetizations of two layers separately. A disadvantage of this method is the fact that MOKE magnetometry does not provide information about the absolute value of the magnetic moment of the sample. On the other hand, since the magnetization is monitored in the region of the focused light beam (30–50 μm), the method provides the possibility of a highly localized analysis of the magnetic properties. This allows [Gru91] a special sample geometry with wedge-type spacers to be used for the measurements. This has the advantage that a continuous range of spacer thicknesses can be studied with a single sample.

VSM magnetometry uses the Faraday induction effect for detecting the magnetic moment of the sample. During the measurements the magnetic sample vibrates with a frequency ω between two pick-up coils. The coils are connected in a such way that the induced voltages, which are proportional to the total magnetic moment of the sample, are added. The total voltage oscillating with the same frequency ω is measured by means of the lock-in technique, which is known to be very sensitive. As an option, one can use three pairs of pick-up coils, so that all three components of the magnetic moment can be measured simultaneously.

SQUID magnetometry is based on the highly sensitive Josephson effect. In this method the magnetic sample is placed in a superconducting coil, which is inductively connected to a contour with a pair of Josephson junctions. The total magnetic flux through the contour can be typically monitored with an accuracy of better than few per cent of the magnetic flux quantum $\Phi_0 = h/2e = 2.07 \times 10^{-7}$ G cm^2. The magnetic moment of the sample is thus measured by measuring the magnetic flux through the coil where the sample is situated.

As has already been mentioned, unlike the MOKE technique, VSM and SQUID magnetometry provide information about the absolute values of the magnetic moment. However, they have no spatial resolution. Therefore they are usually used in combination with MOKE as a calibration method [Rue96].

All the methods described above are sensitive enough to provide the possibility of measuring, for example, the magnetic moment of one monolayer of Fe.

3.1.2. Domain observation. Another possibility for investigating the interlayer coupling is the observation of magnetic domain patterns and their evolution with increasing applied magnetic field. The most common technique, which accomplishes this task, is MOKE microscopy (see [Hub98] and references therein). Similar to MOKE magnetometry, this method can provide information about the magnetization of two or several magnetic layers if their thicknesses are about 10–20 nm. The analysis of complicated domain patterns is based on a comparison of the images taken in the orientations corresponding to different magneto-optical effects (the Kerr effect, the Voigt effect and gradient effects). In this case the determination of the magnetization directions in different domains made by magneto-optical microscopy is unambiguous.

Scanning electron microscopy with polarization analysis (SEMPA) takes advantage of the fact that secondary electrons emitted from a ferromagnetic layer have a spin polarization which is proportional to the layer magnetization. Therefore, if the electrons are excited by a well enough focused electron beam in a scanning electron microscope, one can obtain the spatially resolved magnetization image of the sample. The details of the apparatus can be found in [Pie94] and [Pie94a]. The main difference between SEMPA and magneto-optical microscopy is the surface sensitivity. Actually, only those electrons which are close enough to the surface can escape before losing sufficient energy, that they fall below the vacuum level. The corresponding sampling depth in this case is about 1 nm. Therefore, only the top magnetic film of the layered system is monitored effectively by this technique.

3.1.3. Spin waves monitoring. Both techniques, ferromagnetic resonance(FMR) and Brillouin–Mandelstamm light scattering (BMLS), discussed in this section are used for measuring the frequency of spin wave modes. These techniques are effective tools for detecting interlayer coupling in layered systems, because the spin wave frequencies are very sensitive to the static magnetic configuration. Their field dependences unambiguously reflect the reorientation transitions taking place in the system (for details see [Hil94], [Hei94a], [Coc94]). Moreover, since the interlayer coupling changes the boundary conditions for the spin waves and therefore their frequencies, its value can be measured even if the coupling does not change the orientation of the static magnetizations. Historically, the first observation of antiferromagnetic bilinear coupling was made by means of BMLS in the Fe/Cr/Fe layered system [Gru86], which was magnetically saturated by the external field. Both bilinear and biquadratic coupling can be taken into account by quantum mechanical calculations [Mac94].

The main difference between FMR and BMLS is connected with the different wavevectors of the spin waves under investigation. The excitation conditions of the spin waves are also different in both techniques. For FMR studies the sample is placed in a resonator and spin waves with $k \approx 0$ are to be excited by a microwave generator, operating at a given frequency. The transmitted and/or reflected signal, which indicate the absorption of microwave power in the resonator, are detected as a function of the external field. The absorption should take place if the microwave pumping frequency coincides with the frequency of a particular spin wave mode in the system at a given field. Different modulation techniques are used to improve the sensitivity of the method.

In the BMLS method inelastic scattering of light is used for detecting the frequency of the spin waves modes, which are, as usual, thermally excited. The scattering process can be described as the creation or absorption of a spin wave quantum (magnon) by a photon. The energy (frequency)

changes of the photon correspond to the energy (frequency) of the magnon. This frequency shift is then measured by means of high-resolution spectroscopy. Varying the experimental conditions one can change the wavevector of the magnons to be studied. The typical wavevectors correspond to the wavevectors of visible light and are in the interval of 10^4–10^6 cm^{-1}. Another advantage of BMLS is the possibility of monitoring spin waves in the region of the focused light beam, which can be made as small as 30–50 μm. This allows one to use wedge-type samples and to investigate systems with different film thicknesses just by scanning along the wedge. The main disadvantage of BMLS arises from the relatively low BMLS intensities. BMLS studies of the layered systems, based on magnetic substances with a weak magneto-optical interaction (e.g. Ni), are time-consuming. For the same reason the low-temperature BMLS studies of thin magnetic films are also very questionable. One option is to combine FMR and BMLS techniques. In this case the spin waves are excited by microwave power as in FMR techniques, and are observed by BMLS. Such a technique has been used for the investigation of the interlayer coupling in the wedge-type Fe/Cr/Fe samples [Dem93].

3.2. Experimental examples

Since its experimental discovery in Fe/Cr/Fe(001) and fcc Co/Cu/Co(001) in 1991 biquadratic coupling has been found in many layered systems: Fe/Au/Fe(001) [Fus92], [Koe92], [Mcc93]; Fe/Al/Fe(001) [Fus92], [Mcc93], [Fil93]; Fe/Cu/Fe(001) [Hei93], [Hei94]; NiFe/Ag/NiFe [Rod93], [You96], [Cow96]; Fe/Ag/Fe(001) [Cel93], [Sc95]; Fe/V/Fe [Pou97]; Co/Ru/Co [Zha94], [Zol96]; NiFe/Cu/Co [Tan95]; Co/Cr/Fe [The95]; NiFe/Cu/NiFe [Lea96]; Fe/FeSi/Fe [Ful96], [Sai96]; and Fe/AuSn/FeNiB [Fuc97]. It is impossible to review all mentioned systems. The aim of the present section is to consider some examples which demonstrate the main common features of the effect and are useful for the discussion of the theoretical models.

3.2.1. Fe/Cr/Fe. Since first hints for the existence of biquadratic coupling in Fe/Cr/Fe trilayers were observed [Gru91], [Ung91] and its existence was firmly established [Rue91], [Dem91], the Fe/Cr/Fe system has been investigated in detail [Hei93a], [Pie94], [Ful95], [Elm95], [Mee95], [Sch95], [Gri96], [Hic96], [Aze96]. A variety of experimental techniques have been used to improve the understanding of the origin of the biquadratic coupling in this system. Now it is thought that the coupling phenomena in the Fe/Cr/Fe system essentially depend on the magnetic structure of the Cr spacer, which is in turn very sensitive to the preparation conditions.

A domain pattern obtained by means of MOKE microscopy at $H = 0$ from the Fe/Cr/Fe trilayer for $t_{Cr} = 0.5$ nm (at $t_{Cr} = 0.5$ nm the bilinear coupling changes its sign from the FM type to the AF one and, therefore, its strength is close to zero) and its combination analysis are shown in figure 3, taken from [Rue91]. The important feature of the domain pattern is the mutual orientation of the magnetization of the two Fe layers. As it was discussed in section 3.1.2, MOKE microscopy allows one to separate the contributions from the two layers and, therefore, to determine the magnetization orientations for each layer. A total of eight gray shades were observed with suitable settings. From the whole complex of observations the following conclusions were drawn: (i) the magnetization vectors of the two layers are always perpendicular to each other; (ii) the magnetization of one particular layer in the different domains can be aligned along any of the four easy axes, corresponding to the fourfold magnetic symmetry of Fe(001). The second statement is no less important than the first, and it cannot be derived, for example, from the domain pattern recorded by SEMPA [Ung91], [Pie94]. This results implies that the orientation of the magnetizations is governed by their *mutual interaction* rather than by the uniaxial anisotropies with different orientation of the easy axes for both layers. The third important statement originates from the magnetization curve measurements (see figure 5). As has already been discussed in section 2, the 90° orientation of the two magnetic layers manifests itself in the magnetization curves as a plateau with an easy axis component, which is equal to one-half of the saturation magnetization. Magnetization curves shown in figures 5(*b*) and 5(*c*) demonstrate the fact that such plateaus really exist for Fe/Cr/Fe. The corresponding field intervals of their existence are larger than the coercive field. This means that the observed phase cannot represent some kind of metastable state.

The strength of the biquadratic coupling was measured for samples with different thicknesses of the Fe layers, t_{Fe}, with the thickness of the two magnetic layers being the same [Dem91]. It was found that it is roughly proportional to $1/t_{Fe}$. This fact confirmed the surface origin of the coupling. Finally, the biquadratic coupling was proved to dominate at thicker Cr spacers. This means that the biquadratic coupling strength decreases with increasing Cr spacer thickness much more slowly than the strength of the bilinear one. This feature was later observed in other systems (Fe/Au/Fe, Fe/Al/Fe [Fus92], and Fe/AuSn/FeNiB [Fuc97]).

Although the Fe/Cr/Fe(001) system is ideally suited for the demonstration of biquadratic interlayer coupling, it is hard to determine the strength of the coupling for the whole interval of t_{Cr}, because often (see section 2) it cannot be separated from the bilinear coupling contribution. One attempt to overcome this difficulty and to provide an independent and straightforward determination of both the bilinear and the biquadratic coupling strength from one single experiment was done in [Elm95] and [Sch97] where the Cr/Fe/Cr/Fe/W(110) layered system was studied. It is possible to prepare this system so that both Fe layers have uniaxial anisotropies with orthogonal easy axes in the plane, because the Fe(110)/W(110) interface strongly supports the in-plane [110] easy axis, whereas a Fe(110)/Cr(110) interface supports the bulk in-plane [001] easy axis. Magnetization curves were measured using a MOKE magnetometer. The curves contained parts with smooth changes of the magnetization as well as jumps. The curves were then fitted on the basis of the interlayer coupling expression similar to equation (1.6) with an additional

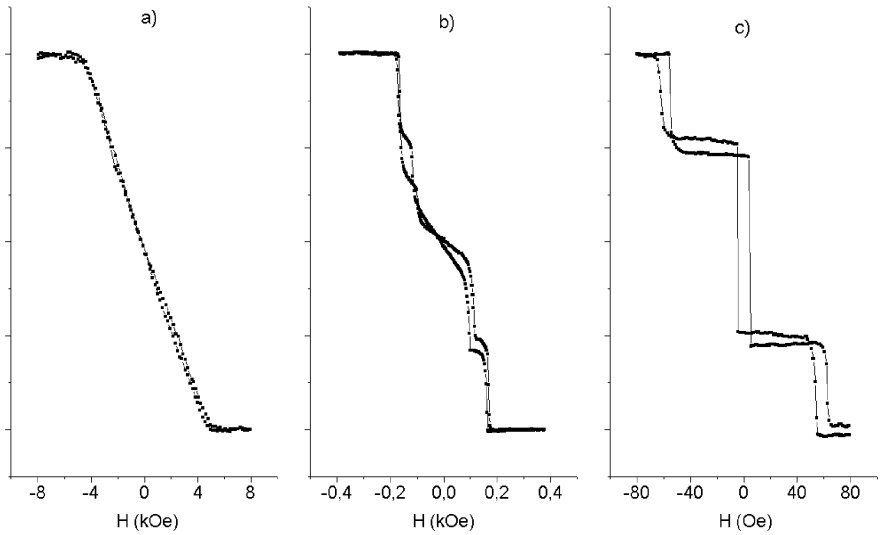

Figure 5. Easy axis magnetization curves of the Fe(3 nm)/Cr, t_{Cr}/Fe(001)(3 nm) layered system measured by MOKE magnetometry: (*a*) t_{Cr} = 0.6 nm, (*b*) t_{Cr} = 2.5 nm, (*c*) t_{Cr} = 3.8 nm. Note the different scales of the magnetic field for the different curves (from [Rue91]).

anisotropy term, describing the uniaxial anisotropies of the Fe layers. The values of J_1 and J_2 were obtained as fit parameters. The results of such a procedure are shown in figure 6. A strong antiferromagnetic extremum of the bilinear coupling at $t_{Cr} = 3.6$–4 monolayers (ML) and the following oscillations are observed in good agreement with the results for the Fe/Cr/Fe(001) system [Gru91]. However, the observed biquadratic coupling was surprisingly strong in contradiction to [Dem91] and [Koe92]. This finding was discussed in [Elm95] and [Sch97] in connection with a fluctuation mechanism, proposed by Slonczewski [Slo91] (see section 4.2). In the frame of this mechanism J_2 is associated with the fluctuation of J_1, caused by the fluctuation of the spacer thickness. Strong biquadratic coupling was attributed to a particular morphology of the interfaces with a long-scale roughness.

A thorough study of the Fe/Cr/Fe(211) trilayers by means of complementary techniques (BMLS, MOKE and SQUID magnetometry) also reveals the increased strength of the biquadratic coupling in comparison with that of the Fe/Cr/Fe(100) system [Gri96].

The temperature dependence of the biquadratic coupling in the Fe/Cr/Fe multilayers was investigated in [Ful95] in connection with the magnetic properties of the Cr spacer. It was shown that the Néel temperature (T_N) of Cr decreases with decreasing thickness in agreement with earlier Mössbauer measurements [Sau91]. The surprising result was that for $t_{Cr} > 6.5$ nm the biquadratic coupling disappeared below T_N of the spacer. The origin of this effect is not clear at present.

3.2.2. Fe/Au/Fe, Fe/Al/Fe. The next systems after Co/Cu/Co and Fe/Cr/Fe where the biquadratic coupling was observed were Fe/Au/Fe and Fe/Al/Fe [Fus92]. The importance of these systems is based on the fact that their biquadratic coupling is not small in comparison with the antiferromagnetic bilinear one in the whole interval of the spacer thicknesses. In the Fe/Al/Fe layers, for example, the bilinear coupling is significantly smaller than the Fe/Cr/Fe system, whereas the biquadratic coupling has roughly the same order of magnitude. Easy axis magnetization curves and the corresponding values of $|J_1|$ and $J_2|$ (taken from [Fus92]) demonstrating this fact are shown in figure 7. For all values of the spacer thicknesses, where J_1 and J_2 can be separated ($|J_1| > |J_2|$), the ratio $|J_2|/|J_1|$is never less than 0.3. On the other hand, similar to the case of Fe/Cr/Fe, the strength of the biquadratic coupling decreases with increasing the spacer thickness much more slowly, than the strength of the bilinear coupling. The biquadratic coupling undoubtedly dominates for the thicker spacers (see figures 7(*d*) and 7(*g*)).

Contrary to [Fus92], where the temperature dependence of J_2 in both Fe/Au/Fe and Fe/Al/Fe systems was observed not to be very strong, the Fe/Al/Fe samples studied in [Gut92] and [Fil93] demonstrated a rapid increase of the coupling strength $|J_2|$ with decreasing temperature. This temperature dependence can be well described by $|J_2| \propto \exp(-T/T_0)$ or $|J_2| \propto (1 - T/T_0)^2$. However, from the comparison of the RHEED patterns published in [Fus92] and [Gut92] one can conclude that the crystallographic quality of the samples in [Fus92] was better, than for the samples investigated in [Gut92]. The connection between the quality of the samples and the temperature dependence of $|J_2|$ is explained by the so-called 'loose spins' model [Slo93], which considers paramagnetic impurities in the interlayer. A detailed discussion of the 'loose spins' model will be given in section 4.3.

3.2.3. NiFe/Ag/NiFe. In this section NiFe-based layered systems, revealing the biquadratic interlayer coupling are

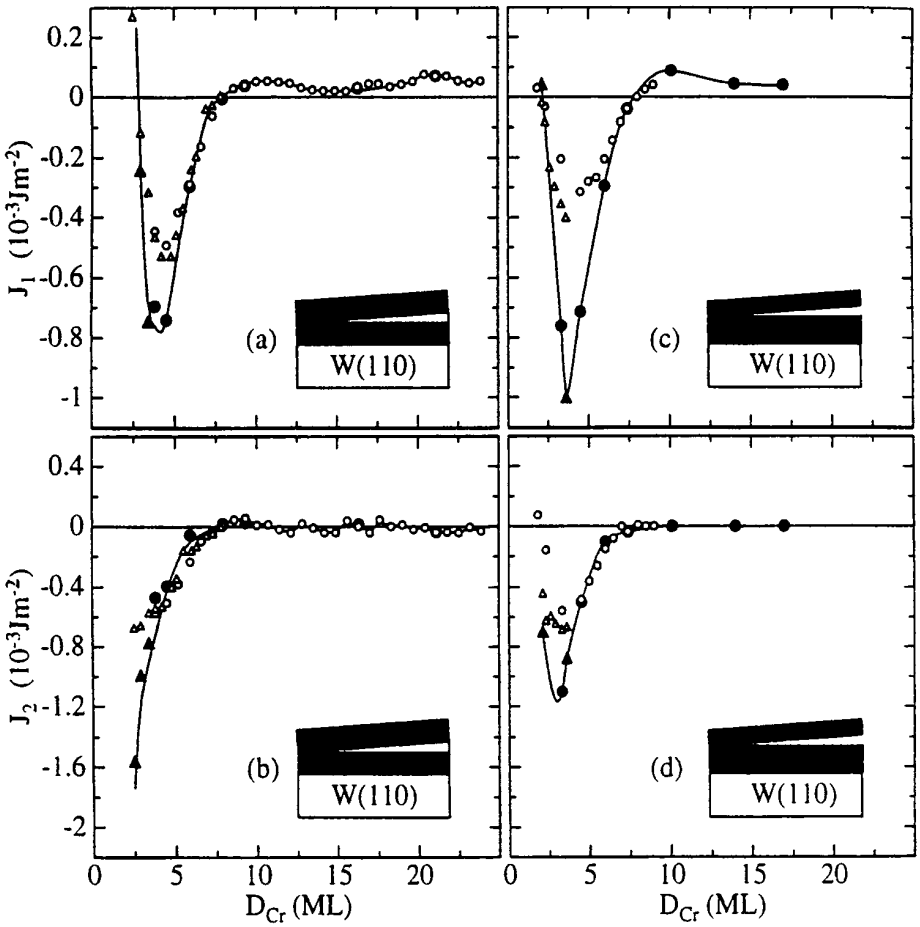

Figure 6. Coupling parameters J_1 and J_2 versus the thickness of the Cr spacer in the Cr/Fe/Cr/Fe/W(110) layered system, shown for samples with Fe layers of the same thickness, t = 20 ML (*a*, *b*) and for samples with Fe layers of different thickness t_1 = 13 ML and t_2 = 25 ML (*c*, *d*) (from [Elm95]).

discussed. Contrary to Fe or Co, NiFe is a ferromagnet with negligible crystallographic anisotropy. Therefore, the phase diagram shown in figure 4 does not describe the ground state of the system consisting of two NiFe layers separated by a non-magnetic spacer, and the behaviour of such a system differs dramatically from the behaviour of Fe(001)-based systems. Although the biquadratic coupling favours the 90° orientation, the system never reaches it in the presence of the additional bilinear coupling. Generally speaking, if $|J_1| < 2|J_2|$, the system is always in a canted phase, the canting angle between two magnetization vectors being determined by equation (2.1). This is demonstrated by the magnetization curves of the NiFe/Ag multilayers shown in figure 8. The samples were prepared by d.c. sputtering. Ag and $Ni_{81}Fe_{19}$ layers, 1.08 nm and 1.22 nm thick respectively, were deposited sequentially onto glass substrates kept at a temperature of 100 K. The full curves in the figure correspond to a fit on the basis of the energy expression given by equation (1.6) with an additional Zeeman energy term. From this fit one obtains not only the equilibrium canting angle between the magnetizations in zero field (it is about 135° at 10 K and reaches 180° above 100 K), but also the parameters determining the strength of the bilinear and the biquadratic couplings (see figure 9). Note that the parameters J and B, which are shown in figure 9, are connected with J_1 and J_2 by $J_1 = JM_S^2$ and $J_2 = 2BM_S^2$, where M_S is the temperature-dependent spontaneous magnetization of the NiFe layers. It is clearly seen from figure 9 that the temperature dependences of J (or J_1) and B (or J_2) are very different. The parameter J was found to be almost temperature independent, whereas the absolute value of the parameter B decreased rapidly with increasing temperature similar to the results of [Gut92].

4. Theoretical models and their experimental verification

In the above sections we have seen that biquadratic coupling it is a general effect, observed in many layered systems. The strength of the coupling, its temperature dependence and its dependence on the thicknesses of the spacer and on the thicknesses of the magnetic layers were carefully measured by means of different experimental techniques. However, contrary to bilinear coupling, which is well understood and can be described in terms of the theories based on the concept of itinerant magnetism (see, for example, [Hat94], [Fer94], [Slo95]), there is no general

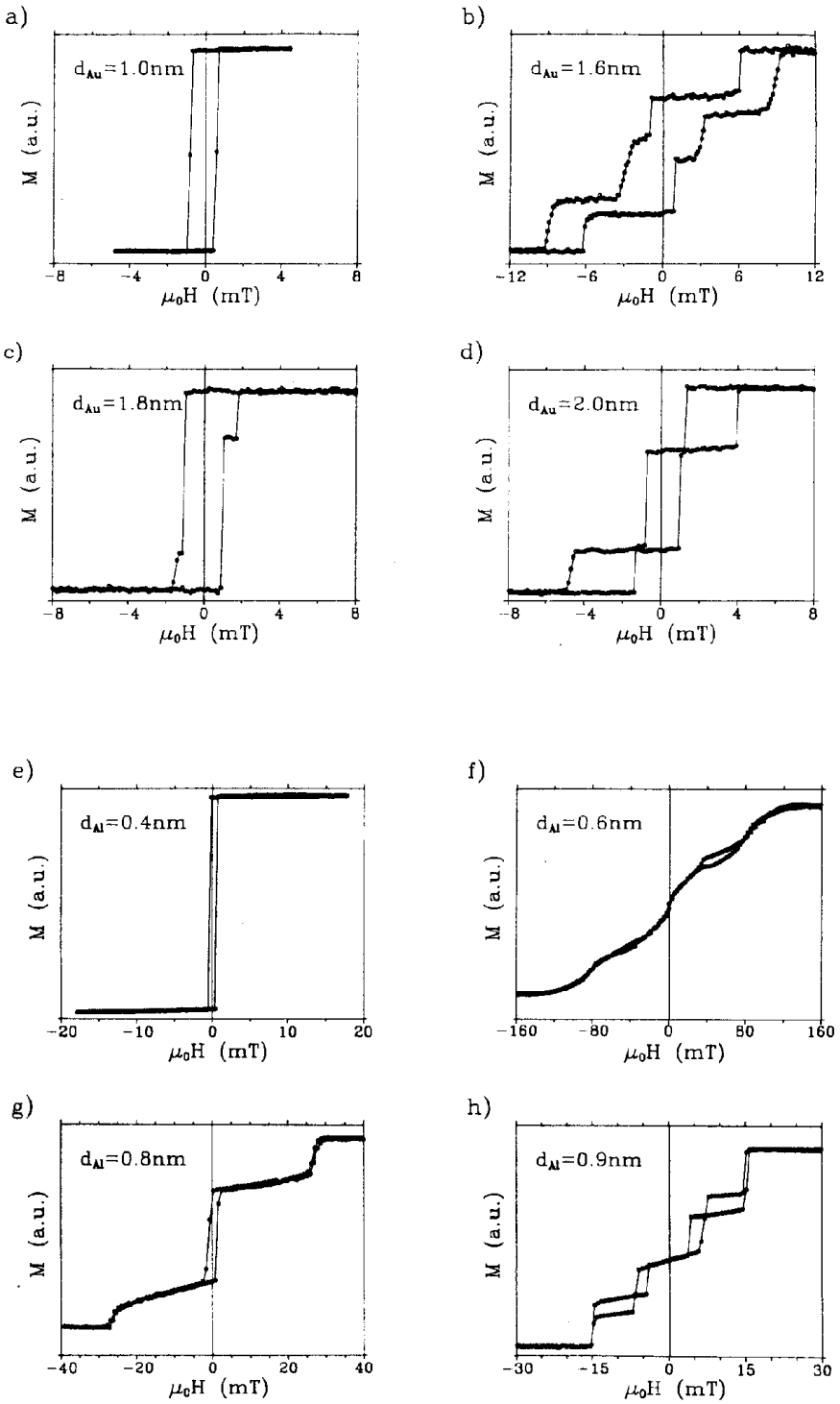

Figure 7. Measured magnetization curves of the Fe/Au/Fe(001) (*a*)–(*d*) and Fe/Al/Fe(001) (*e*)–(*h*) layered systems for the different thicknesses of the Au and Al spacer layers as quoted and the corresponding values of J_1 and J_2: (*a*) $J_1 > 0$, $J_1 + J_2 > 0$; (*b*) $J_1 = -0.014$ mJ m^{-2}, $J_2 = -0.01$ mJ m^{-2}; (*c*) $J_1 + J_2 = -0.001$ mJ m^{-2}; (*d*) $J_1 + J_2 = -0.01$ mJ m^{-2}; (*e*) $J_1 > 0$, $J_1 + J_2 > 0$; (*f*) $J_1 = -0.32$ mJ m^{-2}, $J_2 = -0.16$ mJ m^{-2}; (*g*) $J_1 + J_2 = -0.15$ mJ m^{-2}; (*h*) $J_1 = -0.66$ mJ m^{-2}, $J_2 = -0.28$ mJ m^{-2} (from [Fus92]).

theory for biquadratic coupling, which can be adopted for all systems. In the following sections we consider different models which have been proposed to describe biquadratic coupling in particular systems.

4.1. Intrinsic calculations

First let us discuss so-called intrinsic theories, which consider an ideal layered system without any interface

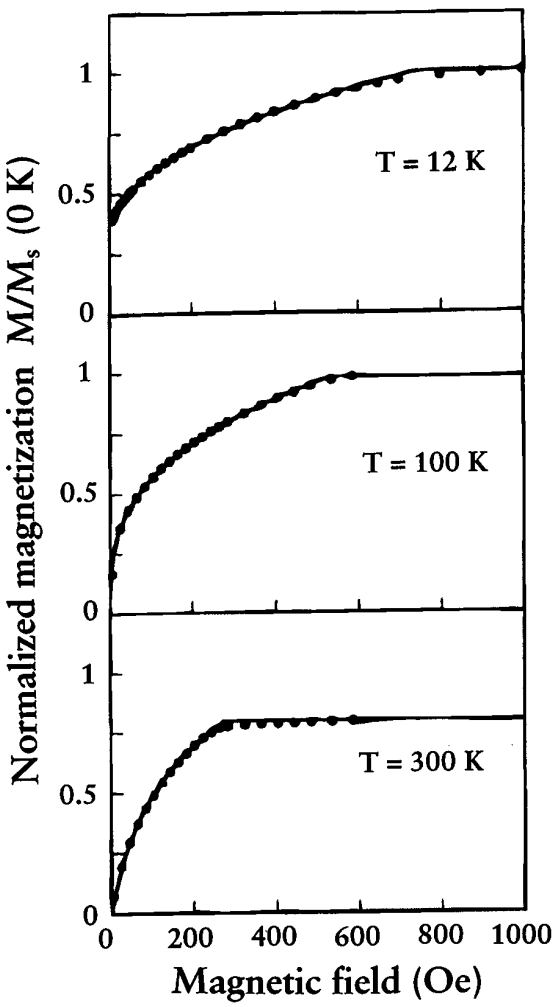

Figure 8. Measured magnetization curves of the NiFe(1.22 nm)/Ag(1.08 nm) multilayer. The data are normalized to the saturation magnetization value at low temperature. The full curves correspond to a fit based on equation (1.6) (from [Rod93]).

roughness and chemical intermixing. There are several calculations of the angular dependence of the intrinsic exchange energy [Eri93], [Edw93], [Bar93], [Ino94], [Spi97] which predict the biquadratic term. In all of these calculations $|J_2|$ was found to be generally much smaller than $|J_1|$ and it was significantly smaller than the values observed experimentally. The theories also predict that J_2 can be a dominating term and thus gives rise to 90° alignment at zero magnetic field only for those spacer thicknesses at which the oscillating parameter J_1 has nodes. This was not observed experimentally. The Fe/Cr/Fe [Dem91], Fe/Au/Fe and Fe/Al/Fe [Fus92], and Fe/Ag/Fe [Cel93] trilayers demonstrated dominating biquadratic coupling for thick spacers. On the other hand, the interpretation of data for the Fe/Cu/Fe system [Hei93] admits the possibility of an appreciable intrinsic contribution to J_2.

4.2. Fluctuation mechanism

Slonczewski [Slo91] attributed the effect of biquadratic coupling to an extrinsic fluctuation mechanism leading to frustration of the bilinear exchange coupling, which can be described as follows. It is well known that in many systems bilinear interlayer coupling oscillates as a function of the spacer thickness with a period of two monolayers (see, for example, [Ung91]), changing its sign if the spacer thickness is changed by one monolayer. Thus, one monolayer high step terraces at the interfaces cause fluctuations of the intrinsic bilinear coupling. If the distance between two one monolayer high steps is not too large (see below), the intralayer exchange stiffness of the ferromagnet resists the torques due to the fluctuations of the interlayer coupling, and the sum of interlayer coupling and exchange-stiffness energies is minimized when the mean moments are orthogonal and an additional static wave of magnetization is formed. The simplest one-dimensional version of the theory yields the following relation for the layered system, containing two equal magnetic layers separated by a spacer (see figure 10):

$$J_2 = -\frac{4(\Delta J_1)^2 L}{\pi^3 A}\coth\left(\frac{\pi D}{L}\right) \qquad (4.1)$$

where A is the exchange stiffness within the two ferromagnetic layers both of thickness D. The spacer has one monolayer high terraces of the width L, at whose edges the local bilinear exchange J_1 has step changes of the amount $\pm\Delta J_1$. The predicted negative sign of J_2 implies that the mechanism always favours the 90° orientation independent of the details of the bilinear interaction. It is also interesting to note that $|J_2|$ increases with L, i.e. as the specimen becomes more 'perfect'. However, if L exceeds the value of a domain wall thickness in the ferromagnet (it is about 50 nm for Fe), the theory breaks down, because the ferromagnetic layers accommodate the changes of J_1 by creating domains with the magnetizations determined by the local values of J_1. On the other hand, the theory is also invalid, if $|J_2| \simeq \Delta J_1$.

There have been a number of experimental verifications of the model. Heinrich *et al* investigated Fe/Cu/Fe(001) trilayers with well-defined interface morphology using FMR and MOKE magnetometry [Hei93]. Thorough crystallographic analysis of the surfaces of the consequent layers showed that the typical terrace width for the samples grown at room temperature was about 6 nm, whereas for the samples grown at elevated temperature it was much larger. The magnetic measurements demonstrated that the biquadratic coupling for the samples grown at elevated temperature is stronger, in agreement with equation (4.1). From measured values of J_1 and J_2 with the help of equation (4.1) the microscopic values of $\Delta J_1(N)$ and thus $J_1(N)$ for N perfectly smooth monolayers of Cu were extracted.

Another study devoted to the fluctuation mechanism was performed by Schäfer *et al*, where the bilinear and biquadratic couplings in the Fe/Ag/Fe(001) trilayers were investigated [Sc95]. Due to the lack of reliable information on the interface roughness of the samples under

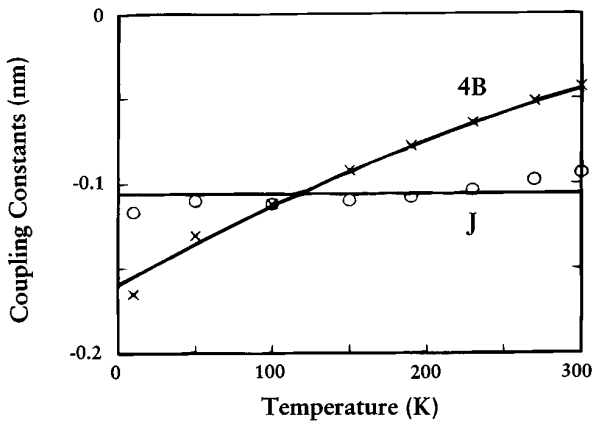

Figure 9. Strengths of the bilinear (J) and biquadratic (B) coupling in the NiFe(1.22 nm)/Ag(1.08 nm) multilayer as a function of temperature. The parameter B is fitted to $B = B_0(1 - T/T_0)^2$ with $T_0 = 630$ K (from [Rod93]).

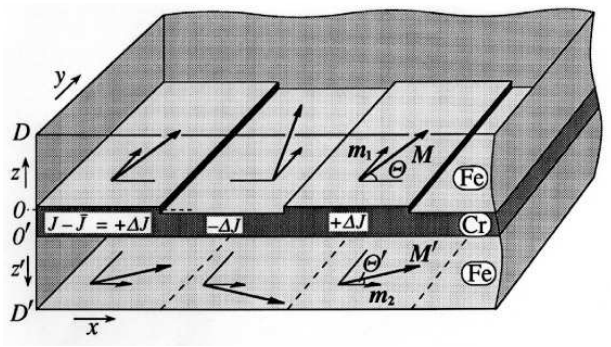

Figure 10. Perspective section of a magnetic trilayer with periodic monolayer high interface terraces. Arrows indicate schematically the continuous pattern of fluctuating static magnetizations $M(x, z)$ and $M'(x, z)$ in the x–y plane due to spatial fluctuations of the bilinear interlayer exchange coupling $J_1(x)$ between the ferromagnetic Fe layers (from [Slo91]).

investigation, it was impossible to use equation (4.1) for direct comparison of J_1 and J_2. However, the temperature dependences of J_1 and J_2 were measured in [Sc95] in a wide temperature interval (4–300 K). Both dependences appeared to be linear:

$$J_1 = J_1^0(1 - \alpha_1 T) \tag{4.2}$$

$$J_2 = J_2^0(1 - \alpha_2 T) \tag{4.3}$$

with $\alpha_1 = 8.8 \times 10^{-4}$ K^{-1} and $\alpha_2 = 1.9 \times 10^{-3}$ K^{-1}. Implying that $\Delta J_1 \propto J_1$ for all temperatures, and using equation (4.1) one can easily obtain that $(\alpha_2/\alpha_1)_{\text{th}} = 2$, which is in a good agreement with the experimentally measured value $(\alpha_2/\alpha_1)_{\text{exp}} = 2.16$. Moreover, using the extrapolated from the experiment values of J_1^0 and J_2^0, a typical terrace length L was estimated from equation (4.1). It is found to be equal to 25 nm. This is in concordance with the STM data obtained for similar samples. Because of the good agreement between the experimental data and the fit made using equation (4.1), the conclusion can be drawn that the fluctuation mechanism accounts for the biquadratic coupling in the Fe/Ag/Fe(001) and Fe/Cu/Fe(001) systems.

4.3. 'Loose spin' model

Strong biquadratic coupling with an unusual temperature dependence in the Fe/Al/Fe trilayers was discussed in section 3.2.2. As seen from previous sections this phenomenon cannot be described by either an intrinsic approach or by the fluctuation mechanism. Slonczewski developed another extrinsic model, called the 'loose spin' model, to explain this effect [Slo93].

The main role in this model is played by magnetic impurities embedded in the spacer. Let us consider two identical saturated semi-infinite ferromagnetic films with the unit magnetization vectors $\boldsymbol{m}_1$ and $\boldsymbol{m}_2$ (see figure 11, taken from [Slo93]). Consider also an additional magnetic atom (or a cluster of atoms) with the local spin S ('loose spin') at the position z somewhere within the spacer. This atom is subjected to the exchange fields $\boldsymbol{U}_1 = U(z) \cdot \boldsymbol{m}_1$ and $\boldsymbol{U}_2 = U(w - z) \cdot \boldsymbol{m}_2$, which are due to the respective conduction-electron polarizations induced by the two ferromagnets. The resulting potential $U^*(\varphi, z)$ can be expressed by

$$U^*(\varphi, z) = |\boldsymbol{U}_1 + \boldsymbol{U}_2| = (U_1^2 + U_2^2 + 2U_1U_2\cos\varphi)^{1/2} \tag{4.4}$$

where, as usual, φ is the angle between $\boldsymbol{m}_1$ and $\boldsymbol{m}_2$. From conventional statistics, the free energy per loose spin is

$$f^{LS}(T, \varphi, z) = -K_BT \times \ln\left(\frac{\sinh[(1 + (2S)^{-1})U^*(\varphi, z)/k_BT]}{\sinh(U^*(\varphi, z)/2Sk_BT)}\right). \tag{4.5}$$

The macroscopic free energy $F^{LS}(T, \varphi,)$ can be obtained from $f^{LS}(T, \varphi, z)$ through integration over all loose spins in the spacer. It represents an additive contribution to the φ-dependent energy coupling of the two ferromagnetic layers. $F^{LS}(T, \varphi)$ depends on φ in quite a complicated way, but it can be expanded in the form

$$F^{LS}(\varphi) = J_0 - J_1^{LS}\cos\varphi - J_2^{LS}\cos^2\varphi + \cdots \tag{4.6}$$

with J_1^{LS} and J_2^{LS} being the strengths of the bilinear and the biquadratic coupling. It is clear from equation (4.5) that the free energy and, correspondingly, J_1^{LS} and J_2^{LS} should possess a strong temperature dependence. In the limit of small loose spin concentrations they are proportional to the concentration. Note here that the loose spins in the spacer are considered in the model as independent. Therefore it is applicable only for small concentrations of magnetic impurities. It is difficult to compare the predictions of the theory with the results from [Fus92] and [Gut92] because the concentration of the impurities and their distribution across the non-magnetic spacer layers were not known. However, the measured temperature dependence of the biquadratic coupling can be described quite well with a reasonable number of fitting parameters.

There is another type of 'loose spins'. These are magnetic atoms, located at the surface of the ferromagnetic metal ($z = 0$ in figure 11). In this case U_1 is determined by an interaction of a surface spin with its neighbours and $U_1 \gg U_2$. It is much more complicated to determine the thermodynamics of these atoms, mainly because of the uncertainty in the interaction of these spins with the bulk ferromagnet [Slo93].

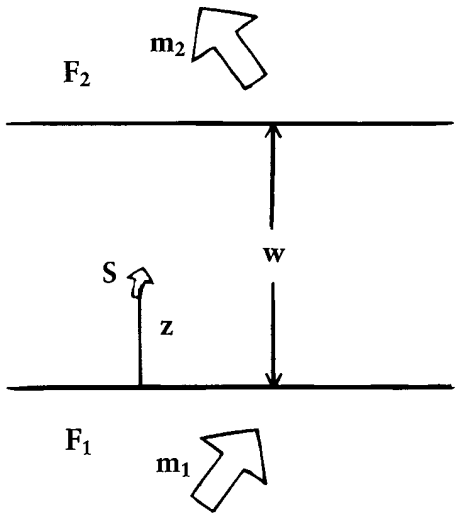

Figure 11. Cross section showing two semi-infinite ferromagnets F_1 and F_2, with unit moments m_1 and m_2, coupled by a non-magnetic spacer of thickness w. The small arrow represents a loose spin S situated at a distance z from F_1 (from [Slo93]).

There are several publications where the experimental examination of the predictions of the loose spin model in Fe/Cu/Fe(001) [Hei94], Co/Cu/Co(001) [Vri95] and Fe/Ag/Fe(001) [Sc95] have been reported. In all cases a layer with a certain concentration of magnetic atoms (Fe or Co) was intentionally inserted at various positions within the non-magnetic spacer. No clear evidence for 'loose spin behaviour' as predicted in [Slo93] was found in [Hei94] or [Vri95], whereas the results of [Sc95] are in a very good agreement with the model. Let us consider the latter work in detail. The design of the Fe/Ag/Fe sample studied in [Sc95] is shown in figure 12. In the middle of the Ag spacer with constant thickness of $t_{Ag} = 1.8$ nm an additional, submonolayer Fe wedge ($t = 0$–0.15 nm) was introduced. Note here that t for submonolayers means an effective thickness, or, what is equivalent, an effective area concentration of atoms. Precautions were taken to reach optimal growth of the sample and to minimize interdiffusion (see [Sc95] for details). The Fe/Ag/Fe trilayer with $t_{Ag} = 1.8$ nm was chosen at the first antiferromagnetic extremum of the interlayer coupling [Cel93] and allowed to separate the parameters J_1 and J_2 in a wide temperature range ($|J_1| > |J_2|$, see section 2), therefore any changes in J_1 and J_2 caused by the additional Fe wedge could be easily observable.

The magnetic properties of the system were examined using static MOKE magnetometry and MOKE microscopy. In both cases the thin Fe wedge did not contribute significantly to the measured signal, therefore the alignment of the magnetic moment of the two thick Fe (1.5 nm) layers were deduced from the measurements. Two transitions were observed for all $M(H)$ curves (compare with equations (2.3) and (2.4)); therefore both J_1 and J_2 were actually determined. For the determination of the Fe thickness interval, where the loose spin model can be applied, the difference between the strengths of the

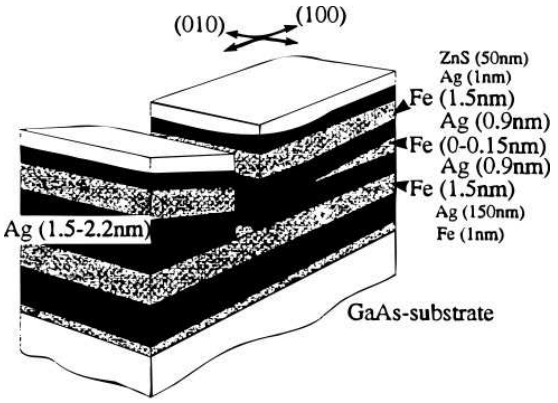

Figure 12. Schematic drawing of the sample used in [Sc95] for the experimental verification of the 'loose spin' model.

biquadratic coupling with and without the additional 'loose spin' Fe layer was measured. It is plotted in figure 13 for $T = 7$ K as a function of the Fe wedge thickness. It is clearly seen that for small Fe concentrations J_2^{LS} increases linearly with the Fe concentration, in agreement with the theory. But for Fe layer thicknesses over $t_l = 0.02$ nm (0.13 ML) the linear dependence breaks down, demonstrating the inapplicability of the model. The interaction between atoms or small atomic clusters becomes significant, and magnetic percolation takes place in the layer. For the investigation of the temperature dependence of the interlayer coupling the magnetic properties of the Fe(1.5 nm)/Ag(0.9 nm)/Fe(0.008 nm)/Ag(0.9 nm)/Fe(1.5 nm) multilayer were studied. The thickness of the middle Fe layer was chosen to be deliberately smaller than t_l. Only under this condition can the loose spin model be used for a description of the experimental results. The results of these measurements are shown in the inset of figure 13. Contrary to the Fe/Ag/Fe system with the presumably pure spacer (see the previous section) J_2^{LS} demonstrates a strong temperature dependence at low temperatures. The full curves in figure 13 are calculated on the basis of equations (4.4) and (4.5) with the same fitting parameters for both curves: $U/k_B = 10$ K (which corresponds to a reasonable value of the bilinear coupling $J_1 = 1$ mJ m^{-2}) and $S = 5S_{Fe}$, where S_{Fe} stands for the spin of an Fe atom. The latter condition means that the Fe atoms form clusters on the Ag surface with five atoms in each cluster on the average.

From the above discussion it is also clear that additional magnetic layers embedded in Cu spacers by Heinrich *et al* and de Vries *et al* (0.5 ML and 1 ML in [Vri95] and 0.25 ML and 0.5 ML in [Hei94]) were too thick to be well described by the loose spin model.

4.4. Magnetic-dipole mechanism

The third extrinsic mechanism of the biquadratic coupling takes into account the dipole fields created by rough interfaces in the layered system [Dem94]. It was shown earlier by computer simulations that for the ideal surface the dipole field is spatially periodic with the lattice

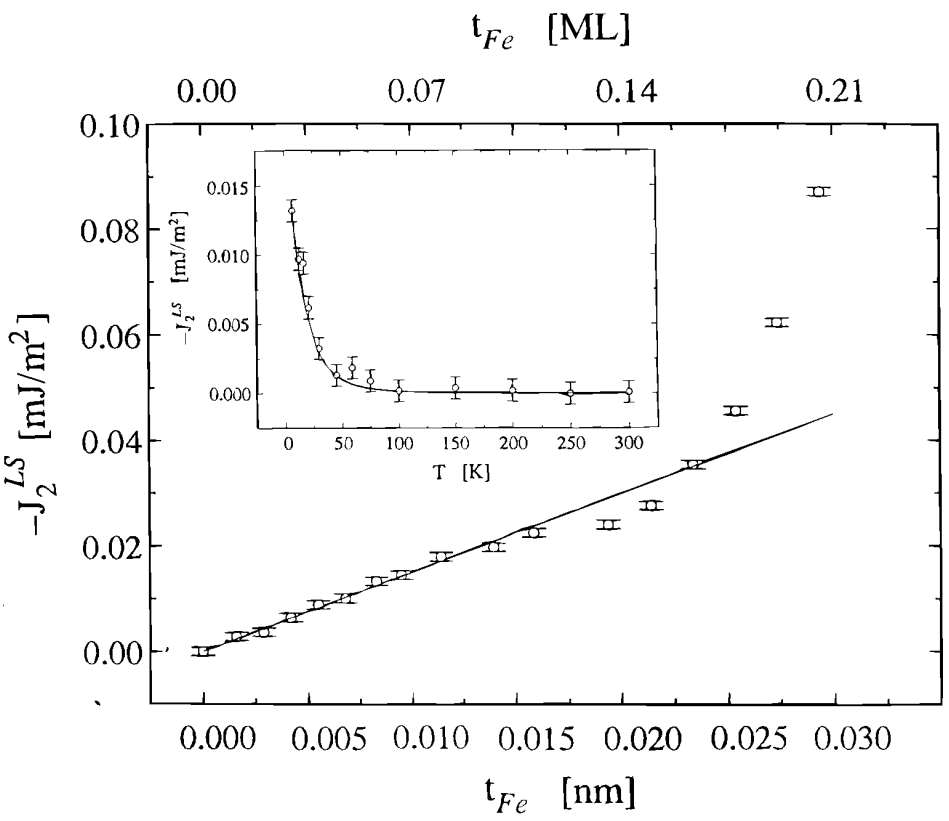

Figure 13. Difference between the strengths of the biquadratic coupling for the Fe/Ag/Fe(001) layered systems with and without an additional Fe layer (J_2^{LS}), measured at T = 7 K as a function of the thickness of this layer (t_{Fe}). The inset shows the temperature dependence of J_2^{LS} at t_{Fe} = 0.06 ML. The full curves, are fits on the basis of the 'loose spin' model (from [Sc95]).

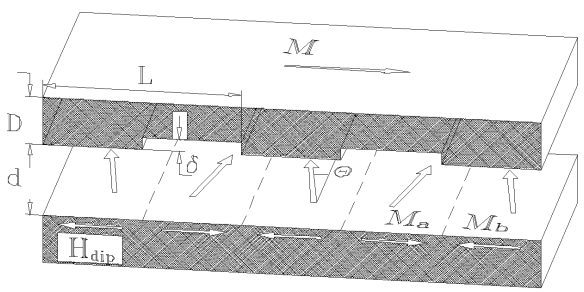

Figure 14. Perspective section of two magnetic films separated by a spacer. Both magnetic films have equal thicknesses D, while the thickness of the spacer layer is d. The upper film is supposed to have periodic interfacial terraces with period L and height δ. The bottom film is assumed to have a smooth interface.

constant and vanishes exponentially with distance from the surface [Hei88], the exponential decay being determined by the lattice constant as well. Therefore, even at a distance of 1–2 ML from the ideal surface the dipole field becomes negligibly small and cannot be responsible for any interlayer coupling. However, the interface roughness causes the dipole field which decreases with distance from the surface more slowly than in the case of the ideal surface. If the roughnesses of the two films are not correlated, one can take them into account separately. For simplicity let us suppose that the surface of one ferromagnetic film has an array of infinitely long growth terraces and valleys with a period L, the second film having a smooth surface. Figure 14 illustrates the situation under consideration. The x-projection of the dipole field, created by such a structure can be written as follows

$$H_{\mathrm{dip}}(x,z) = -\frac{8\pi M\delta}{L}\sum_{m=1}^{\infty}(-1)^{m-1}\cos\left(\frac{2\pi}{L}(2m-1)x\right) \times \exp\left(-\frac{2\pi}{L}(2m-1)z\right) \tag{4.7}$$

where δ and L are the height and a periodicity of the roughness structure and M is the uniform magnetization of the magnetic film (the x, y, z-axes are defined in figure 10). It is clear from equation (4.7) that the smooth film is situated in a dipole field potential, *oscillating* along the x-direction, which is induced by the rough film. The exchange stiffness of the film resists the local torques caused by the oscillating potential, and the sum of the interlayer coupling and the exchange-stiffness energies is minimized when the mean moment of the film is orthogonal to the direction of the dipole field (which is in its turn parallel to the magnetization of the rough film), and an additional static wave of magnetization is formed. Although the dipole fields are mainly concentrated in the surface region ($H \propto \exp(-z/L)$), the interaction caused by the dipole fields, strictly speaking, is not a pure

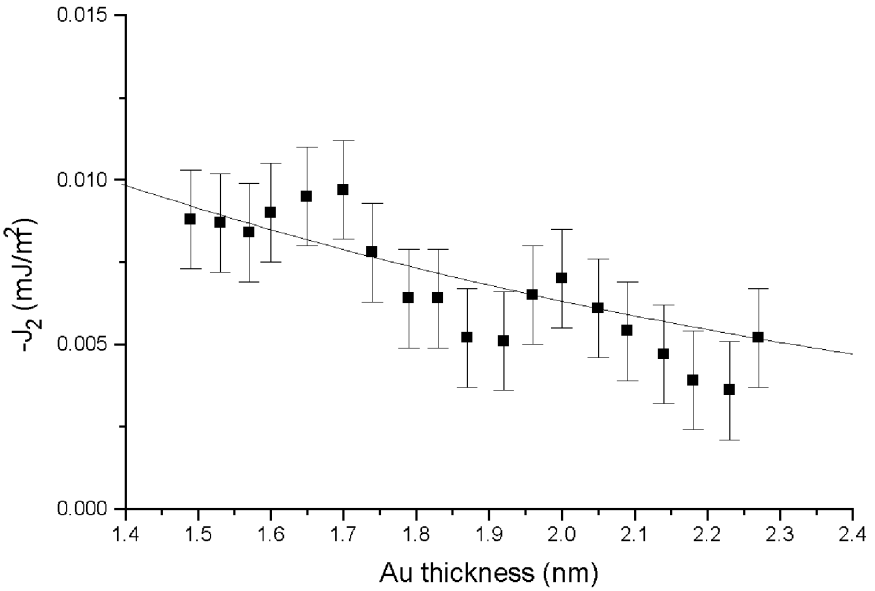

Figure 15. Interlayer biquadratic coupling strength J_2 for the Fe/Au/Fe(001) layered system induced by the interface roughness as a function of the thickness of the spacer layer. Full squares represent the difference between the interlayer coupling of the rough sample and the average value of that for the smooth one. The full curve is a result of calculations based on the magnetic-dipole mechanism for $L = 17$ nm, $\delta = 0.8$ nm (from [Rue95]).

interfacial one. However, one can introduce the surface interaction parameter J_2 with the dimensionality of mJ m^{-2} by integrating the bulk coupling strength over the magnetic film thickness. Taking into account that the roughnesses of both interfaces of the two films provide independent contributions to J_2 one obtains

$$J_2 = -\frac{M^4\delta^2 L}{\pi A}\sum_{m=1}^{\infty}\frac{(-1)^{m-1}}{(2m-1)^3}\exp\left(-\frac{4\pi d}{L}(2m-1)\right) \times\left[1-\exp\left(-\frac{8\pi D}{L}(2m-1)\right)\right]. \tag{4.8}$$

From equation (4.8) it becomes obvious that the strength of the coupling depends on the characteristic scale L and the height δ of the interface roughness. Typical data, obtained from the STM studies of the Fe films grown on Ag [Bue97] are $L = 20$–50 nm and $\delta = 0.5$–1 nm. In this case J_2 is of the order of 0.01 mJ m^{-2}. An important feature of the mechanism under discussion is that the strength of the coupling is independent of the spacer material, but it depends on the film roughness.

Note also here that laterally varying dipole fields created by interface roughness can also lead to the bilinear magnetostatic coupling [Nee62], if one assumes the correlated roughness of both interfaces (e.g. 'orange peel' structure).

The experimental verification of this mechanism was performed in [Rue95]. The interlayer coupling for two kinds of Fe/Au/Fe(001) layered structures were examined using MOKE and SQUID magnetometry. The samples were prepared either at room temperature or at $T = 80\,^{\circ}$C on the Ag buffer based on the GaAs(001) substrate [Gru91]. It was shown that the elevated deposition temperature caused almost perfect interfaces with negligible roughness. On the other hand, the interfaces of the samples prepared at room temperature possessed considerable roughness, which was studied by STM [Bue97]. The difference between the biquadratic coupling strengths measured for these two systems was considered to be due to the rough interfaces of the sample prepared at room temperature. This difference is plotted in figure 15 as a function of the Au layer thickness. The full curve is calculated in terms of the magnetic-dipole model using the roughness parameters known from independent STM measurements. The agreement between the theory and the experimental results leads to the conclusion that the magnetic-dipole mechanism determines the biquadratic coupling in the Fe/Au/Fe(100) layered system with considerable roughness.

The exchange coupling between amorphous ferromagnetic FeNiB and a polycrystalline Fe layer across amorphous AuSn spacer was studied in [Fuc97]. At a spacer thickness of 3 to 5 nm the magnetization direction of the top Fe layer changed continuously from parallel to 90° alignment (relative to the magnetization of FeNiB) and remained in its perpendicular orientation for the AuSn spacer up to at least 10 nm. It was possible to describe the experimental results with help of the magnetic-dipole mechanism using the roughness parameters extracted from STM studies.

5. Conclusions

This review paper might be concluded by adding some general remarks on the phenomenon of biquadratic interlayer coupling. It was shown that different experimental techniques were used for investigation of the biquadratic coupling. Since the experimental discovery of this effect in 1991 biquadratic coupling has been observed in many layered systems. In some systems it dominates, in some cases it is relatively weak. However, the fact is that

the biquadratic coupling is a general phenomenon, inherent to exchange coupled magnetic layers. Several theoretical models have been developed which were proved to describe the effect properly. Nevertheless, contrary to the situation with the bilinear coupling, there is no general theory which can be adopted for all systems.

Two important points, related to the discussed subject, remain beyond the scope of this review article. The first is a non-collinear magnetic arrangement, observed in Fe/Cr multilayers [Sch95] and in CoFe/Mn/CoFe-trilayers [Kre96], which is thought to be due to the exchange stiffness *in non-ferromagnetic spacers* [Slo95]. Such an interaction cannot be described as a biquadratic one, although it also causes a non-collinear ground state of the layered magnetic system.

The second point, which has not been discussed in this paper, is a connection between biquadratic coupling and the giant magnetoresistance effect (GMR) (see, for example, [Cow96], [Kum96], [Pet97]). GMR describes the magnetoresistance of layered systems correlated with the change in the arrangement of the magnetizations of the individual layers [Bai88], [Bin89]. Currently a high GMR effect with a low saturation field was observed in layered systems with dominating biquadratic interlayer coupling [Tan96], which are used for producing high-density rigid magnetic memory disks.

Acknowledgments

The author gratefully acknowledges valuable discussions with A Hubert, U Gradmann, B Hillebrands, P Grünberg and J Slonszewski.

References

[Aze96] Azevedo A, Chesman C, Rezende S M, de Aguiar F M, Bian X and Parkin S S P 1996 *Phys. Rev. Lett.* **76** 4837
[Bai88] Baibich M N, Broto J M, Fert A, Nguyen-Van-Dau F, Petroff F, Etienne P, Creuzet G, Friederich A and Chazelas J 1988 *Phys. Rev. Lett.* **61** 2472
[Bar93] Barnas J and Grünberg P 1993 *J. Magn. Magn. Mater.* **121** 326
[Bin89] Binasch G, Grünberg P, Saurenbach F and Zinn W 1989 *Phys. Rev.* B **39** 4828
[Bue97] Bürgler D E, Schmidt C M, Schaller D M, Meisinger F, Hofer R and Guentherodt H J 1997 *Phys. Rev.* B **56** 4149
[Cel93] Celinski Z, Heinrich B and Cochran J F 1993 *J. Appl. Phys.* **73** 5966
[Coc94] Cochran J F 1994 *Ultrathin Magnetic Structures II* ed B Heinrich and J A C Bland (Berlin: Springer) p 222
[Cow96] Cowache C, Dieny B, Chambered A, Benizri D, Berthet F, Auffret S, Giacomoni L and Nossov S 1996 *Phys. Rev.* B **53** 15027
[Dem91] Demokritov S O, Wolf J A, Grunberg P and Zinn W 1991 *Magnetic Surfaces, Thin Films, and Multilayers Symposium* ed S S P Parkin *et al* (Pittsburgh, PA: Materials Research Society) p 133
[Dem93] Demokritov S O 1993 *J. Magn. Magn. Mater.* **126** 291
[Dem94] Demokritov S O, Tsymbal E, Grünberg P, Zinn W and Schuller I K 1994 *Phys. Rev.* B **49** 720
[Dem98] Demokritov S O, Tsymbal E, Bauer M and Hillebrands B to be published
[Edw93] Edwards D M, Ward J M and Mathon J 1993 *J. Magn. Magn. Mater.* **126** 380
[Elm95] Elmers H J, Liu G, Fritzsche H and Gradmann U 1995 *Phys. Rev.* B **52** 696
[Eri93] Erickson R P, Hathaway K B and Cullen J R 1993 *Phys. Rev.* B **47** 2626
[Fer94] Fert A and Bruno P 1994 *Ultrathin Magnetic Structures II* ed B Heinrich and J A C Bland (Berlin: Springer) p 82
[Fil93] Filipkowski M E, Gutierrez C J, Krebs J J and Prinz G A 1993 *J. Appl. Phys.* **73** 5963
[Fil94] Filipkowski M E, Gutierrez C J, Krebs J J and Prinz G A 1994 *J. Appl. Phys.* **76** 7090
[Fil95] Filipkowski M E, Krebs J J, Prinz G A and Gutierrez C J 1995 *Phys. Rev. Lett.* **75** 1847
[Fuc97] Fuchs P, Ramsperger U, Vaterlaus A and Landolt M 1997 *Phys. Rev.* B **55** 12546
[Fuj95] Fujiwara H 1995 *IEEE Trans. Magn.* **31** 4112
[Ful95] Fullerton E E, Riggs K T, Sowers C H, Bader S D and Berger A 1995 *Phys. Rev. Lett.* **75** 330
[Ful96] Fullerton E E and Bader S D 1996 *Phys. Rev.* B **53** 5112
[Fus92] Fuss A, Demokritov S O, Grünberg P and Zinn W 1992 *J. Magn. Magn. Mater.* **103** L221
[Gri96] Grimsditch M, Kumar S and Fullerton E E 1996 *Phys. Rev.* B **54** 3385
[Gru86] Grünberg P, Schreiber R, Pang Y, Brodsky M B and Sowers H 1986 *Phys. Rev. Lett.* **57** 2442
[Gru91] Grünberg P, Demokritov S O, Fuss A, Vohl M and Wolf J A 1991 *J. Appl. Phys.* **69** 4789
[Gut92] Gutierrez C J, Krebs J J, Filipkowski M E and Prinz G A 1992 *J. Magn. Magn. Mater.* **116** L305
[Hat94] Hathaway K B 1994 *Ultrathin Magnetic Structures II* ed B Heinrich and J A C Bland (Berlin: Springer) p 45
[Hei88] Heinrich B, Purcell S T, Dutcher J R, Cochran J F and Arrott A S 1988 *Phys. Rev.* B **38** 12879
[Hei91] Heinrich B, Cochran J F, Kowalewski M, Kirschner J, Celinski Z, Arrott A S and Myrtle K 1991 *Phys. Rev.* B **44** 9348
[Hei93] Heinrich B, Celinski Z, Cochran J F, Arrott A S, Myrtle K and Purcell S T 1993 *Phys. Rev.* B **47** 5077
[Hei93a] Heinrich B, From M, Cochran J F, Liao L X, Celinski Z, Schneider C M and Myrtle K 1993 *Magnetic Ultrathin Films. Multilayers and Surfaces, Interfaces and Characterization Symposium* ed B T Jonker *et al* (Pittsburgh, PA: Materials Research Society) p 119
[Hei94] Heinrich B, Celinski Z, Liao L X, From M and Cochran J F 1994 *J. Appl. Phys.* **75** 6187
[Hei94a] Heinrich B 1994 *Ultrathin magnetic structures II* ed B Heinrich and J A C Bland (Berlin: Springer) p 195
[Hic96] Hicken R J, Daboo C, Gester M, Ives A J R, Gray S J and Bland J A C 1996 *Thin Solid Films* **275** 199
[Hil94] Hillebrands B and Güntherodt G 1994 *Ultrathin Magnetic Structures II* ed B Heinrich and J A C Bland (Berlin: Springer) p 258
[Hub98] Hubert A and Schäfer R 1998 *Magnetic Domains* (Berlin: Springer)
[Ino94] Inoue J 1994 *J. Magn. Magn. Mater.* **136** 233
[Koe92] Köbler U, Wagner K, Wiechers R, Fuss A and Zinn W 1992 *J. Magn. Magn. Mater.* **103** 269
[Kre96] Krebs J J, Prinz G A, Filipkowski M E and Gutierrez C J 1996 *J. Appl. Phys.* **79** 4525
[Kum96] Kume M, Maeda A, Tanuma T and Kirokik 1996 *J. Appl. Phys.* **79** pt 2B, 6402
[Lea96] Leal J L and Kryder M H 1996 *J. Appl. Phys.* **79** 2801
[Mac94] Maccio M, Pini M G, Politi P and Rettori A 1994 *Phys. Rev.* B **49** 3283
[Mcc93] McCord J, Hubert A, Schäfer R, Fuss A and Grünberg P 1993 *IEEE Trans. Magn.* **29** 2735

[Mee95] Meersschaut J, Dekoster J, Schad R, Belien P and Rots M 1995 *Phys. Rev. Lett.* **75** 1638
[Nee62] Néel L 1962 *C.R. Acad. Sci., Paris* **255** 1545
[Pet97] Pettit K, Gider S, Parkin S S P and Salamon M B 1997 *Phys. Rev.* B **56** 7819
[Pie94] Pierce D T, Unguris J and Celotta R J 1994 *Ultrathin Magnetic Structures II* ed B Heinrich and J A C Bland (Berlin: Springer) p 117
[Pie94a] Pierce D T, Stroscio J A, Unguris J and Celotta R J 1994 *Phys. Rev.* B **49** 14 564
[Pou97] Poulopoulos P, Osberg P, Platow W, Wisny W, Farle M, Hjoervarsson B and Baberschke K 1997 *J. Magn. Magn. Mater.* **170** 57
[Rib92] Ribas R and Dieny B 1992 *Phys. Lett.* **167A** 103
[Rod93] Rodmacq B, Dumesnil K, Mangin P and Hennon M 1993 *Phys. Rev.* B **48** 5077
[Rue91] Rührig M, Schäfer R, Hubert A, Mosler R, Wolf J A, Demokritov S O and Grünberg P 1991 *Phys. Status Solidi* a **125** 635
[Rue95] Rücker U, Demokritov S O, Tsymbal E, Grünberg P and Zinn W 1995 *J. Appl. Phys.* **78** 387
[Rue96] Rücker U, Demokritov S O, Arons R R and Grünberg P 1996 *J. Magn. Magn. Mater.* **156** 269
[Sai96] Saito Y, Inomata K and Yusu K 1996 *Japan. J. Appl. Phys.* **35** L100
[Sau91] Sauer C, Landes J, Zinn W and Ebert H 1991 *Magnetic Surfaces, Thin Films, and Multilayers Symposium* ed S S P Parkin *et al* (Pittsburgh, PA: Materials Research Society) p 153
[Sc95] Schäfer M, Demokritov S O, Müller-Pfeiffer S O, Schäfer R, Schneider M, Grünberg P and Zinn W 1995 *J. Appl. Phys.* **77** 6432
[Sch95] Schreyer A, Ankner J F, Zeidler T, Zabel H, Majkrzak C F, Schäfer M and Grünberg P 1995 *Europhys. Lett.* **32** 595
[Sch97] Schwabenhausen J, Dürkop T and Elmers H-J 1997 *Phys. Rev.* B **55** 15 119
[She96] Shender E F and Holdsworth P C W 1996 *Phys. Rev. Lett.* **76** 2583
[Slo91] Slonczewski J C 1991 *Phys. Rev. Lett.* **67** 3172
[Slo93] Slonczewski J C 1993 *J. Appl. Phys.* **73** 5957
[Slo94] Slonczewski J C 1994 *J. Appl. Phys.* **75** 6474
[Slo95] Slonczewski J C 1995 *J. Magn. Magn. Mater.* **150** 13
[Spi97] Spisak D and Hafner J 1997 *J. Magn. Magn. Mater.* **168** 257
[Tan95] Tanuma T, Takahashi S, Maeda A, Kume M and Kuroki K 1995 *IEEE Trans. Magn.* **31** 3955
[Tan96] Tanuma T, Maeda A, Tatezono F, Kume M and Matono N 1996 *Sanyo Techn. Rev.* **28** 90
[The95] Theis-Brohl K, Scheidt R, Zeidler T, Schreiber F, Zabel H, Mathieu T, Mathieu C and Hillebrands B 1995 *Magnetic Ultrathin Films, Multilayers and Surfaces. Symposium* ed E E Marinero *et al* (Pittsburgh, PA: Materials Research Society) p 165
[Ung91] Unguris J, Celotta R J and Pierce D T 1991 *Phys. Rev. Lett.* **67** 140
[Vri95] de Vries J J, Strijkers G J, Johnson M T, Reinders A and de Jonge W J M 1995 *J. Magn. Magn. Mater.* **148** 187
[You96] Young S, Dieny B, Rodmacq B, Mouchot J and Vaudaine M H 1996 *J. Magn. Magn. Mater.* **162** 38
[Zha94] Zhang Z, Zhou L, Wigen P E and Ounadjela K 1994 *Phys. Rev. Lett.* **73** 336
[Zol96] Zoll S, Van den Berg H A M, Jay J P, Elmers H J, Meny C, Panissod P, Stoeffler D, Dinia A and Ounadjela K 1996 *J. Magn. Magn. Mater.* **156** 231